Supplementary material for 'Current reversal leads to regime change in Amery Ice Shelf cavity in the twenty-first century'

Jing Jin[1, a], Antony J. Payne[1, a], and Christopher Y. S. Bull[2]

[1]School of Geographical Sciences, University of Bristol, Bristol, UK
[2]Department of Geography and Environmental Sciences, Northumbria University, Newcastle Upon Tyne, UK
[a]now at: Department of Earth, Ocean and Ecological Sciences, University of Liverpool, Liverpool, UK

S1 Tuning of tidal velocity

The value of prescribed tidal velocity (U_t) in our simulations was determined based on the results from a sensitivity experiment, in which we modelled the melt rate in 2006 by increasing the tidal velocity from 0 cm/s to 12 cm/s in increments of 2.5 cm/s. The melt rate is increased with the increase in tidal velocity (Figure S1a). Figure S1b suggest that the modelled melt rate with tidal velocity of 2.5, 5 and 7.5 cm/s falls within the observational range (Wen et al., 2010; Yu et al., 2010; Depoorter et al., 2013; Rignot et al., 2013; Herraiz-Borreguero et al., 2016; Adusumilli et al., 2020; Rosevear et al., 2022). To a different extent, the three runs overestimate the melt rate north of the grounding line and underestimate the melt rate at the grounding line (not shown). This is the limitation of our configuration. The relatively coarse resolution cannot represent the steep meridional distributions of basal melting. In addition, Rosevear et al. (2022) estimated the magnitude of typical tidal current under Amery Ice Shelf from four tidal constituents. The estimated magnitude is 9.8 cm/s, which yielded an annual-mean Amery melt rate of 1.1 m/yr in 2006. This is slightly higher than the observational estimate. Considering the tidal velocity of 2.5 cm/s is much smaller than the observed tidal velocity, and 7.5 cm/s might largely overestimate the future melt rate given a very high climate sensitivity of UKESM1.0, we decided to use 5 cm/s.

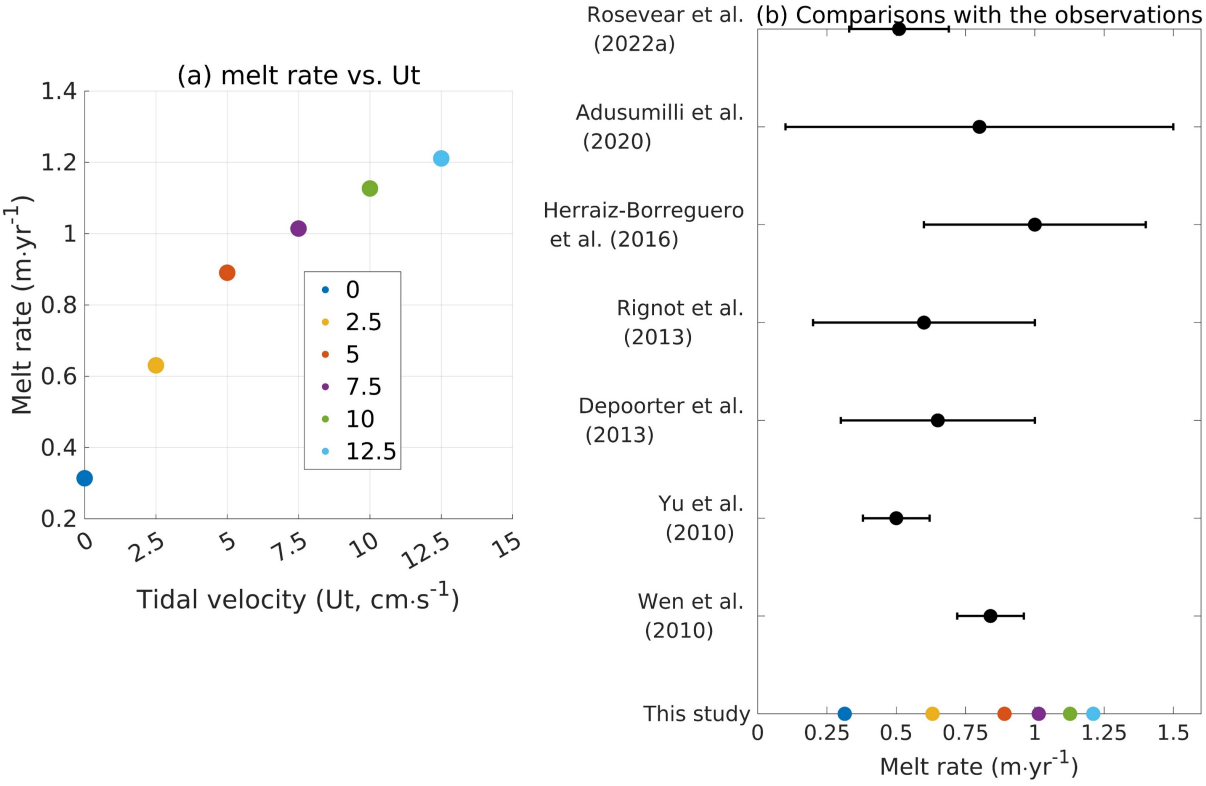

Figure S1. (a) Melt rate against tidal velocity (U_t). (b) Comparison of the melt rate with different U_t with the observational studies.

S2 Supplementary figures for the SSP1-2.6 run forced by the r1i1p1f2 ensemble member

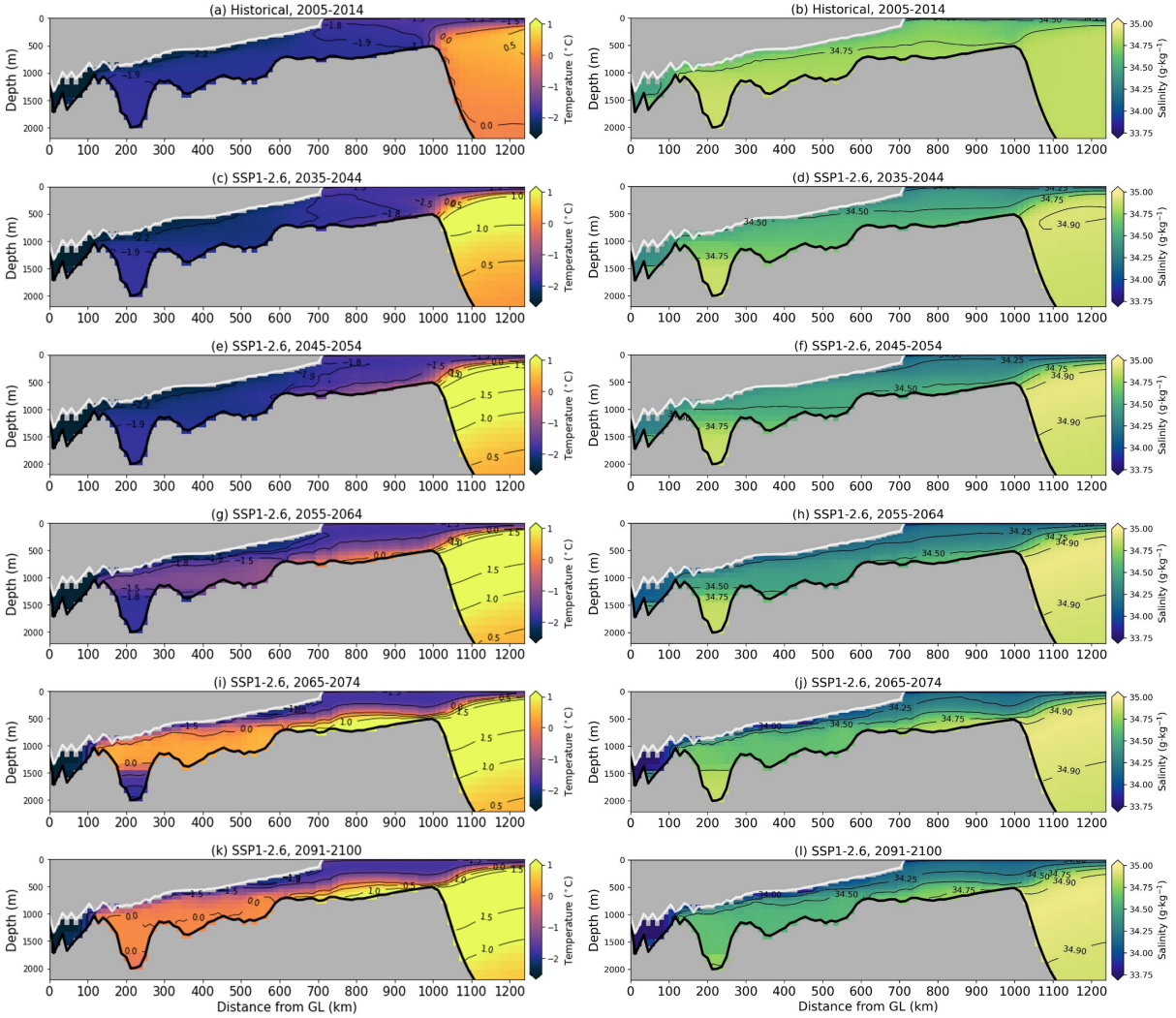

Figure S2. Time-mean of temperature, salinity at a transect extending from the grounding line (GL), Prydz Bay Gyre and the shelf break under SSP1-2.6 scenario. The coordinates show the distance from GL against the depth below sea level. The location of the transect is shown by the white line in Figure 1. The years of the time-mean are shown in the title of each panel.

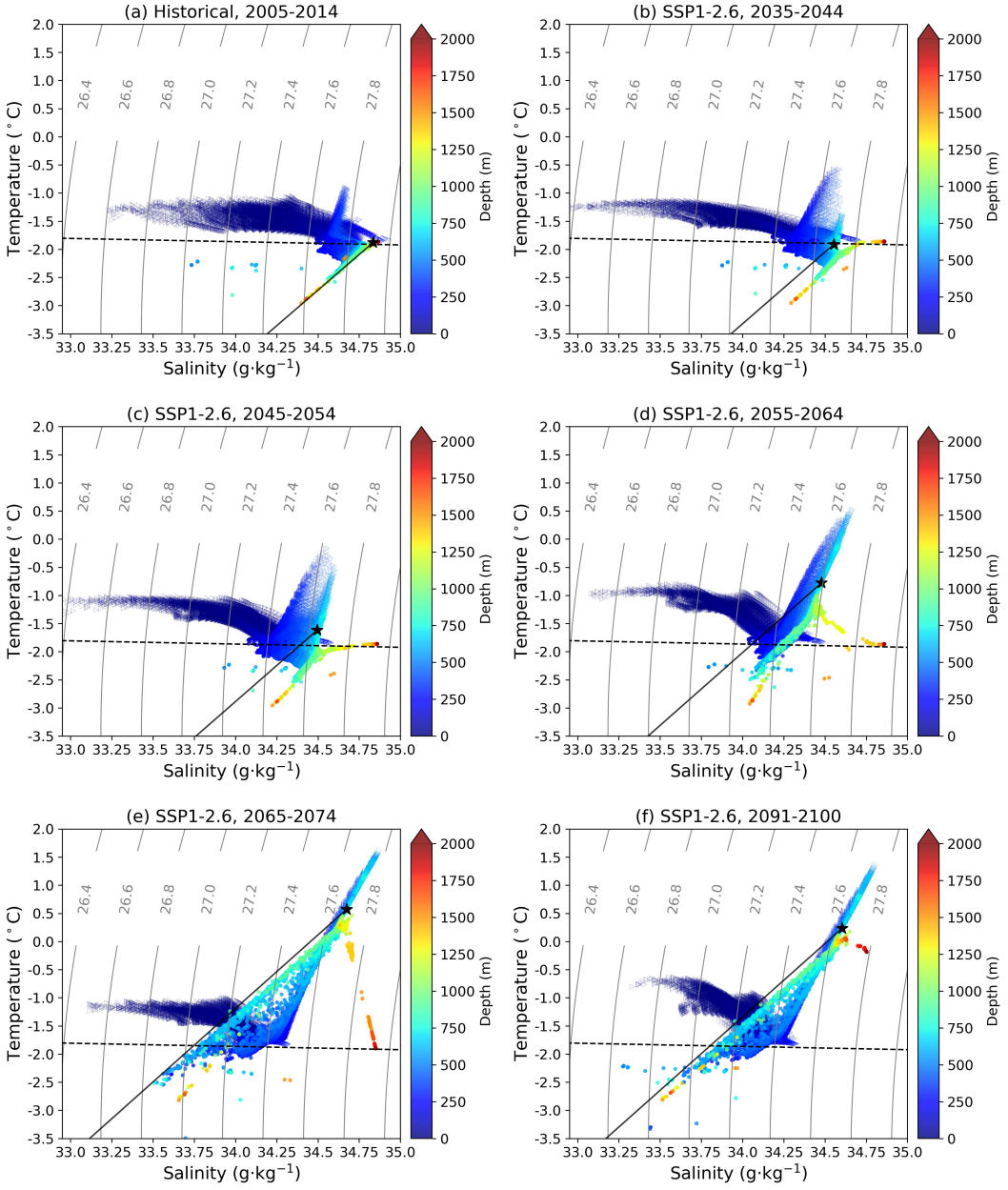

Figure S3. Time-mean of temperature against salinity diagram for each grid cell within the ice shelf cavity (the solid dots) and on the continental shelf (the open triangles) under the SSP1-2.6 scenario. The grey solid lines are potential density. The black dashed line shows the surface freezing point. The black solid line represents the Gade line, defined by end members of the temperature and salinity of the warmest water mass (the black pentacle). The colour schemes show the depth of each grid cell. The years of the time-mean are shown in the title of each panel.

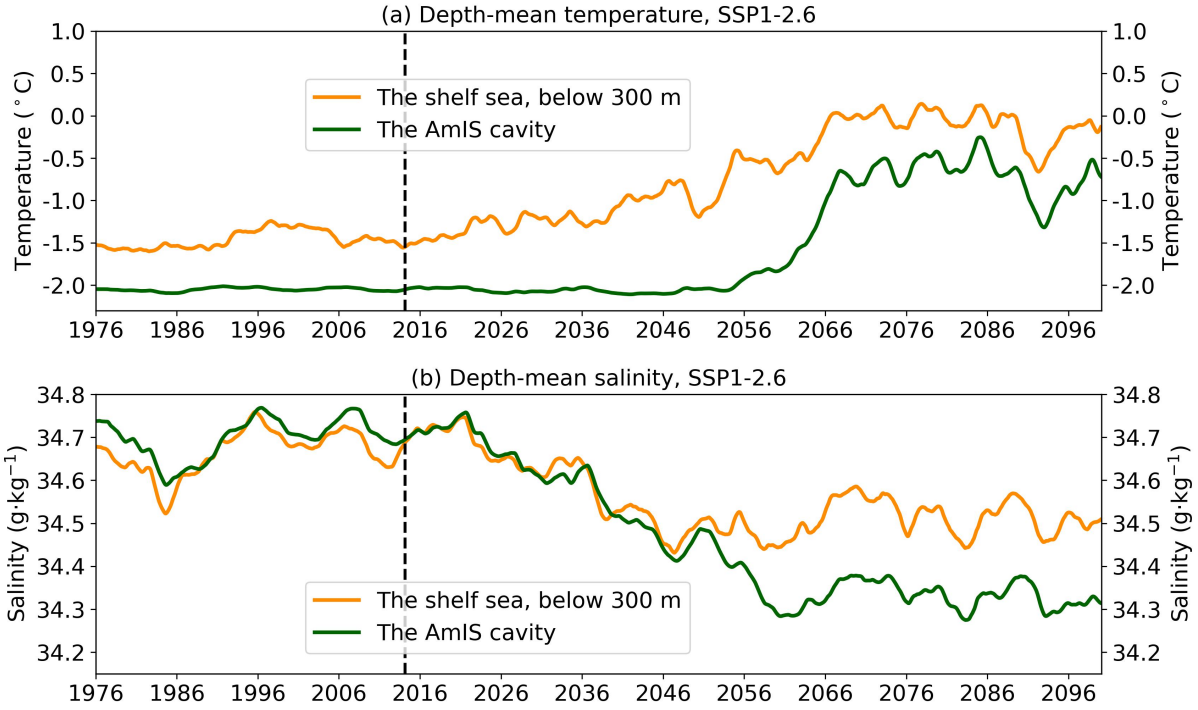

Figure S4. Timeseries of depth-mean (a) temperature and (b) salinity averaged within the ice shelf cavity (the green line) and on the continental shelf below 300 m (the orange line) under the SSP1-2.6 scenario. The vertical dashed line indicates the year of 2015. A 12 month running average is applied.

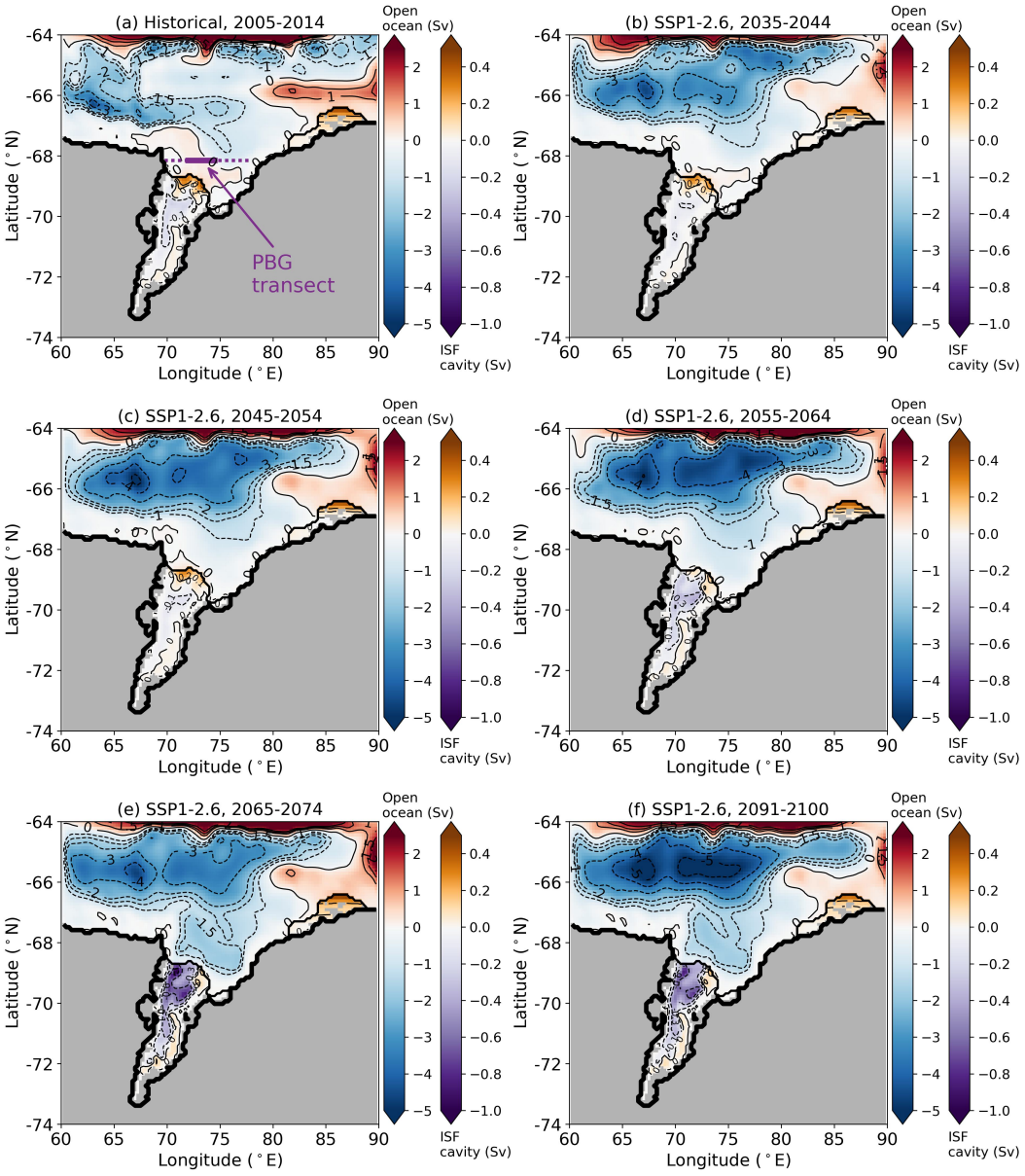

Figure S5. Time-mean of barotropic streamfunction (BSF, in units of Sv) under the SSP1-2.6 scenario. The red-blue colour schemes are for BSF on the open ocean. The values of BSF contours on the open ocean are -5, -4, -3, -2, -1.5, -1, 0, 1, 1.5, 2 Sv. The orange-purple colour schemes are for BSF in the ice shelf cavities. The values of BSF contours in the cavities -0.9, -0.6, -0.3, -0.1, 0, 0.1, 0.2 Sv. The positive/negative BSF represent anti-clockwise/clockwise circulation. The solid and dotted purple line shows the PBG transect and the extended transects to the coasts. The years of the time-mean are shown in the title of each panel.

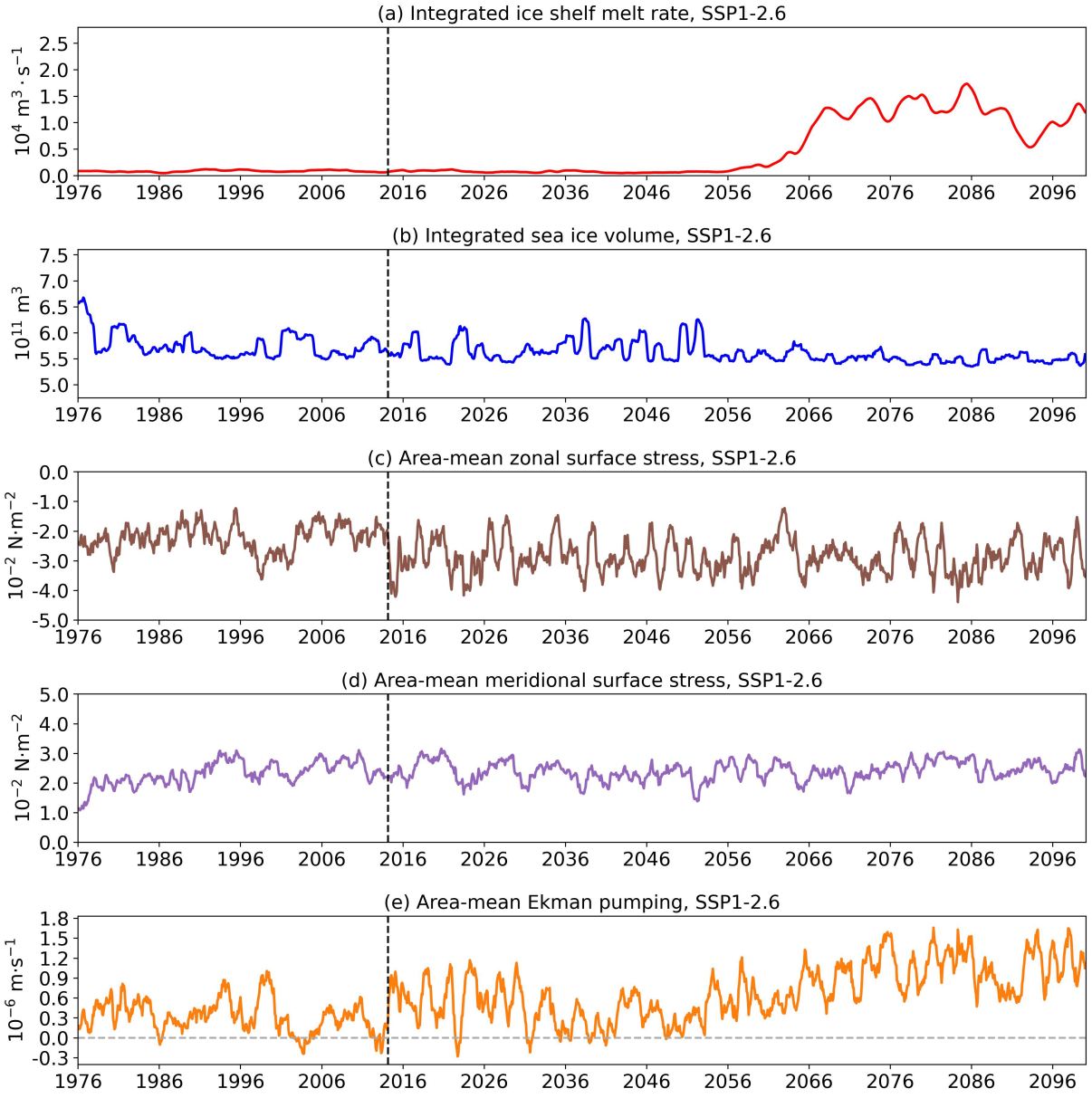

Figure S6. Timeseries of (a) integrated ice shelf freshwater fluxes (10^4 m·s^{-3}), (b) integrated volume of sea ice on the continental shelf (10^{11} m^3), (c) area-mean zonal surface stress within the PBG area (10^{-2} N·m^{-2}), (d) area-mean meridional surface stress within the PBG area (10^{-2} N·m^{-2}), (e) area-mean Ekman pumping within the PBG area (10^{-6} m·s^{-1}) under the SSP1-2.6 scenario. The PBG area is defined using the closed BSF contour of -1.5 Sv in front of the ice shelf in Figure 7f. The vertical dashed line indicates the year of 2015. A 12 month running average is applied.

S3 Supplementary figures for the r2i1p1f2 ensemble member

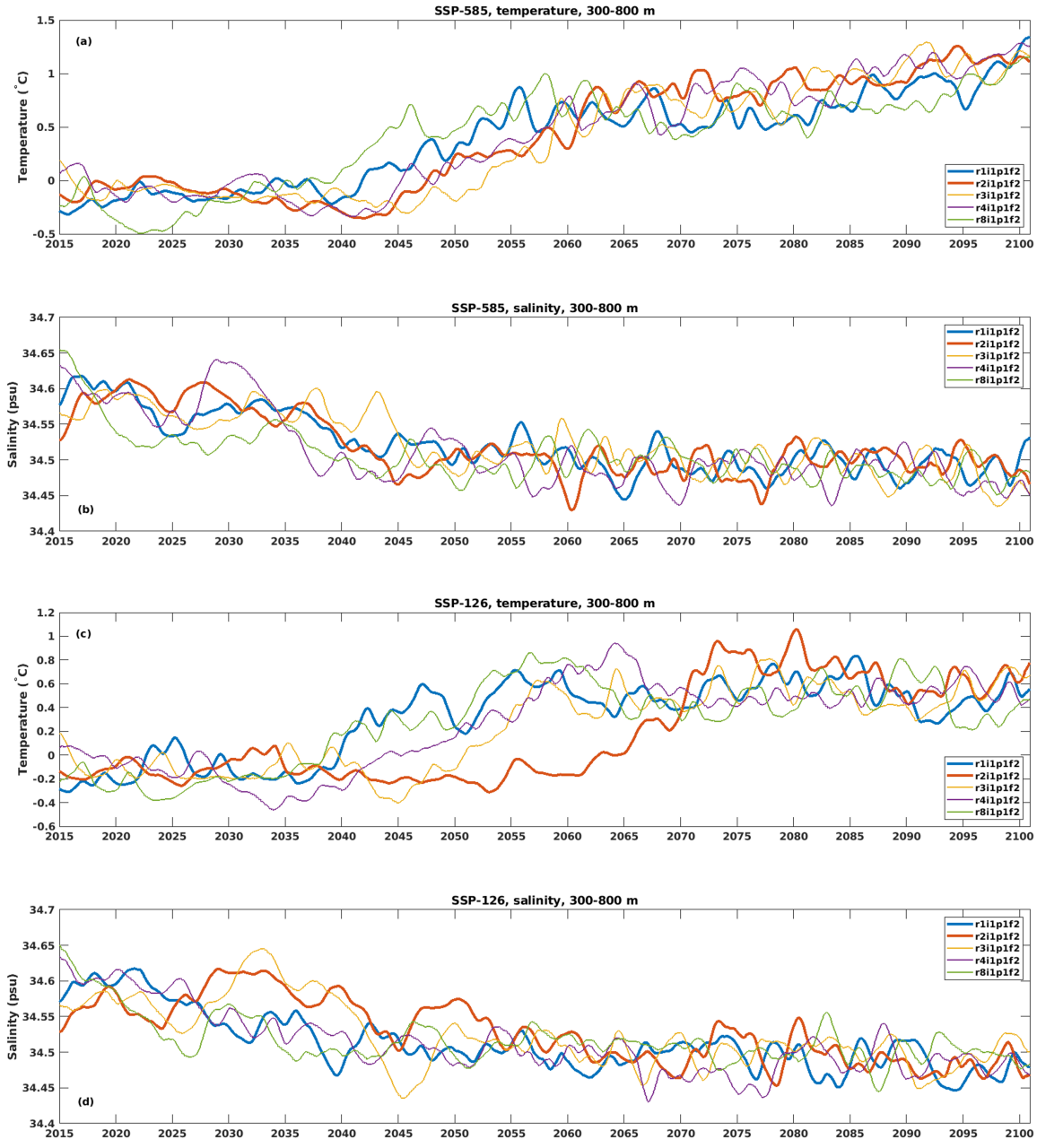

Figure S7. Timeseries of area-mean of mid-depth temperature and salinity within Prydz Bay across five UKESM1.0-LL ensemble members under the SSP5-8.5 and SSP1-2.6 scenario. Note the temperature difference between the r1 and r2 (the thicker lines).

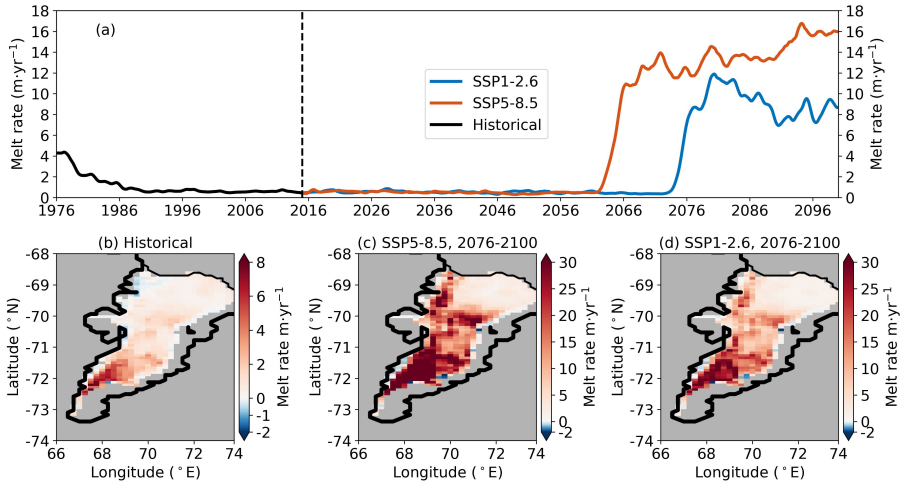

Figure S8. The r2-AME025 results. (a) Time series of the area-averaged melt rate ($\mathrm{m \cdot yr^{-1}}$) from 1976 to 2100. A 12-month-running-average is applied. The dashed vertical line indicates the start of 2015. The time-averaged basal melting over the period of (b) 1976-2014 (Historical), (c) 2076-2100 under SSP5-8.5, (d) 2076-2100 under SSP1-2.6. The warm/cold colours represent melting/refreezing, respectively. Note the different colormap ranges. The colormap for (c) is saturated.

To exclude the abrupt increase in melt rate and the regime change not due to the instability of the model itself, we conducted a second series of experiments forced by the r2i1p1f2 ensemble member of UKESM1.0-LL. Figure S7 shows the comparisons of area-mean mid-depth temperature and salinity within Prydz Bay across five ensembles under the SSP5-8.5 and SSP1-2.6 scenarios. Temperature and salinity changes under the SSP5-8.5 scenario across the ensembles are similar (Figure S7a, b). What is striking is the temperature under the SSP1-2.6 scenario for the r2 ensemble (The thick red line, Figure S7c). The increase in temperature for the r2 ensemble starts in the 2050s-2060s, approximately 20 years later than the temperature increase in the r1 ensemble, which starts in the 2030s (Figure S7c)). Therefore, we chose the r2 ensemble as the forcing of the second series of the AME025 simulations (hereafter the r2-AME025 simulations).

Figure S8 shows that the AmIS melt rate under the SSP1-2.6 scenario from the r2-AME025 simulation behaves similarly to that from the r1-AME025 simulation (Figure 3). However, the timing of the increase occurs later, which coincides with the temperature differences between the r1 and r2 UKESM1.0-LL ensembles. The time evolution of the shelf sea temperature and the cavity temperature under the SSP1-2.6 scenario (Figure S9), and the time evolution of the properties at the PBG transect under the SSP1-2.6 scenario (Figure S9) behave in the same way as the AmIS melt rate. This suggests that the variability of AmIS melt rate and PBG is ultimately controlled by the oceanic forcing, especially the temperature forcing.

In addition, the abrupt increase in the melt rate, the delayed warming in the cavity, the reversed salinity/density gradients between PBG and its western regions and the reversal of PBG are seen in the r2-AME025 simulations under both scenarios (Figure S8-S12). This supports our main conclusions that the freshening-driven PBG reversal causes the regime change in the AmIS cavity.

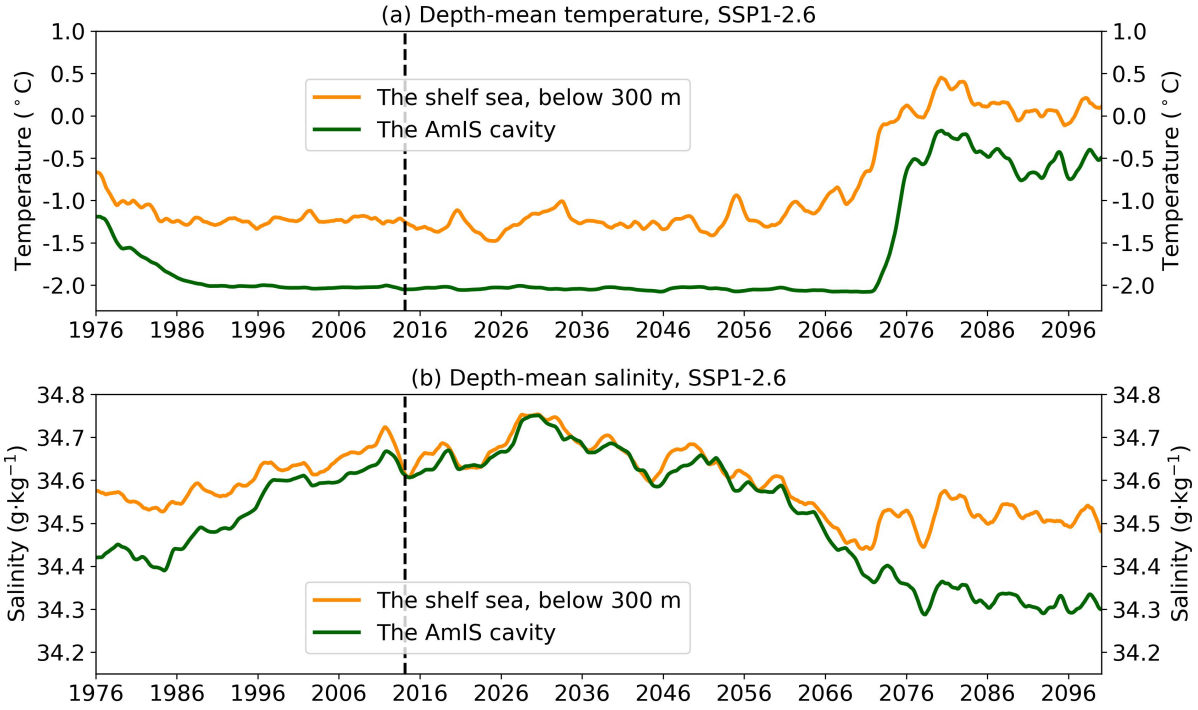

Figure S9. The r2-AME025 results. The outputs are taken from the SSP1-2.6 run. Timeseries of depth-mean (a) temperature and (b) salinity averaged within the ice shelf cavity (the green line) and on the continental shelf below 300 m (the orange line). The vertical dashed line indicates the year of 2015. A 12 month running average is applied.

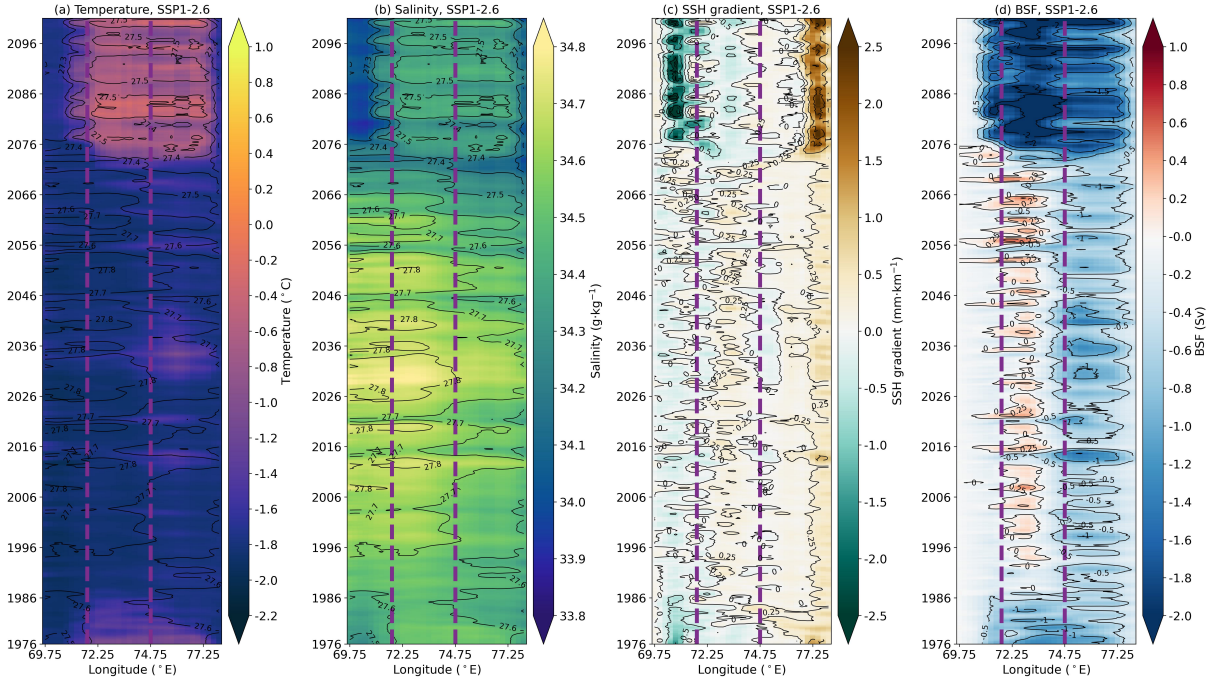

Figure S10. The r2-AME025 results. Hovemoller diagram of properties at the zonal transect shown in Figure 7a. The outputs are taken from the SSP1-2.6 run. (a) Depth-mean temperature below 300 m. (b) Depth-mean salinity below 300 m. The potential density below 300 m overlies temperature and salinity. The values of potential density contours are 27.3, 27.4, 27.5, 27.6, 27.7, 27.8 kg·m^{-3}. (c) Zonal sea surface height gradients (SSH gradient). A positive/negative SSH gradient indicates that the SSH in the east is higher/lower than in the west. The values of SSH gradient contours are -3, -2.5, -1.5, -0.5, 0, 0.25, 1, 2 mm·km^{-1}. (d) Barotropic streamfunction (BSF). The values of BSF contours are -2.5, -2, -1.5, -1, -0.5, 0, 0.25, 0.5, 1 Sv. A positive/negative BSF represents anti-clockwise/clockwise circulation. The transect in between the purple dashed lines is the PBG transect shown by the solid purple line in Figure 7a. A 12 month running average is applied.

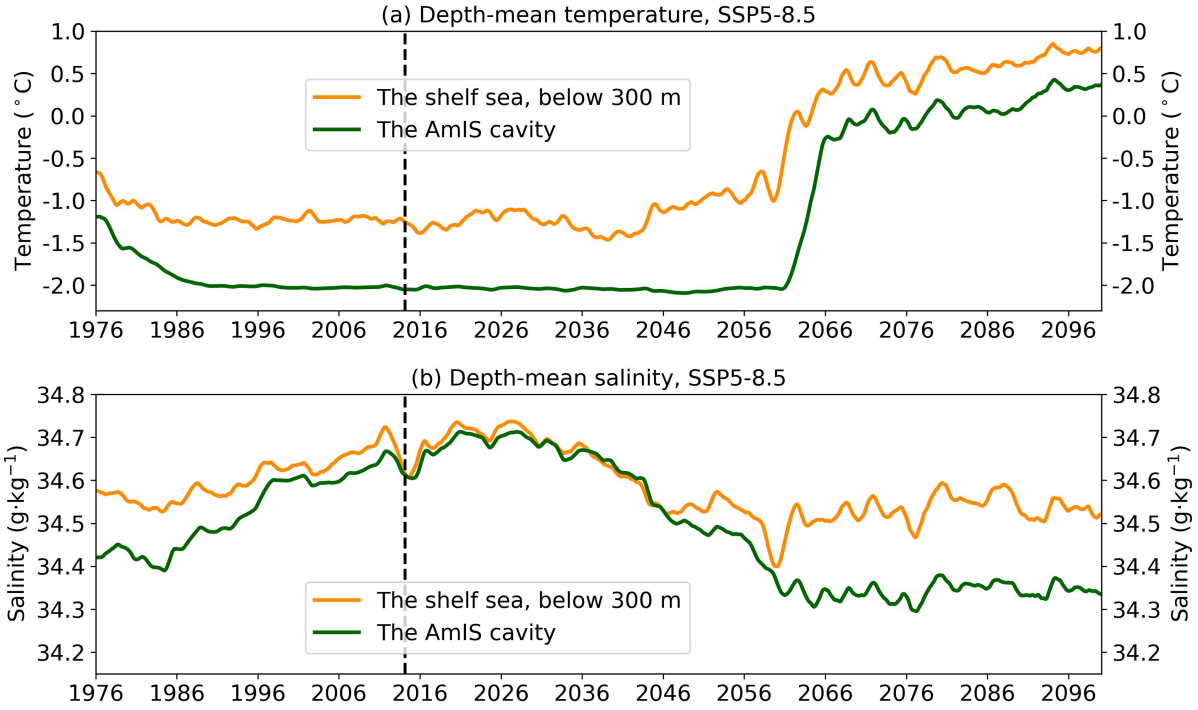

Figure S11. The r2-AME025 results. The outputs are taken from the SSP5-8.5 run. Timeseries of depth-mean (a) temperature and (b) salinity averaged within the ice shelf cavity (the green line) and on the continental shelf below 300 m (the orange line). The vertical dashed line indicates the year of 2015. A 12 month running average is applied.

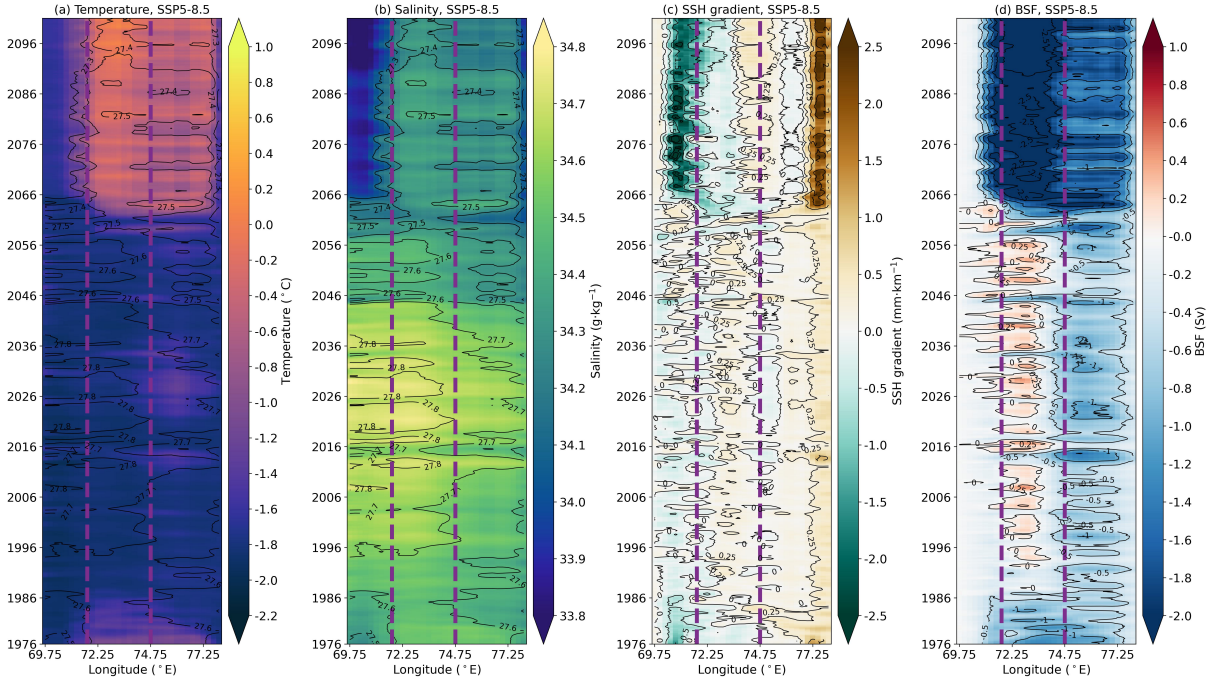

Figure S12. The r2-AME025 results. Hovemoller diagram of properties at the zonal transect shown in Figure 7a. The outputs are taken from the SSP5-8.5 run. (a) Depth-mean temperature below 300 m. (b) Depth-mean salinity below 300 m. The potential density below 300 m overlies temperature and salinity. The values of potential density contours are 27.3, 27.4, 27.5, 27.6, 27.7, 27.8 kg·m^{-3}. (c) Zonal sea surface height gradients (SSH gradient). A positive/negative SSH gradient indicates that the SSH in the east is higher/lower than in the west. The values of SSH gradient contours are -3, -2.5, -1.5, -0.5, 0, 0.25, 1, 2 mm·km^{-1}. (d) Barotropic streamfunction (BSF). The values of BSF contours are -2.5, -2, -1.5, -1, -0.5, 0, 0.25, 0.5, 1 Sv. A positive/negative BSF represents anti-clockwise/clockwise circulation. The transect in between the purple dashed lines is the PBG transect shown by the solid purple line in Figure 7a. A 12 month running average is applied.

References

Adusumilli, S., Fricker, H. A., Medley, B., Padman, L., and Siegfried, M. R.: Interannual variations in meltwater input to the Southern Ocean from Antarctic ice shelves, NATURE GEOSCIENCE, 13, 616+, https://doi.org/10.1038/s41561-020-0616-z, 2020.

Depoorter, M. A., Bamber, J. L., Griggs, J. A., Lenaerts, J. T. M., Ligtenberg, S. R. M., van den Broeke, M. R., and Moholdt, G.: Calving fluxes and basal melt rates of Antarctic ice shelves, NATURE, 502, 89+, https://doi.org/10.1038/nature12567, 2013.

Herraiz-Borreguero, L., Church, J. A., Allison, I., Peña-Molino, B., Coleman, R., Tomczak, M., and Craven, M.: Basal melt, seasonal water mass transformation, ocean current variability, and deep convection processes along the Amery Ice Shelf calving front, East Antarctica, Journal of Geophysical Research: Oceans, 121, 4946–4965, https://doi.org/https://doi.org/10.1002/2016JC011858, 2016.

Rignot, E., Jacobs, S., Mouginot, J., and Scheuchl, B.: Ice-Shelf Melting Around Antarctica, SCIENCE, 341, 266–270, https://doi.org/10.1126/science.1235798, 2013.

Rosevear, M., Galton-Fenzi, B., and Stevens, C.: Evaluation of basal melting parameterisations using in situ ocean and melting observations from the Amery Ice Shelf, East Antarctica, Ocean Science, 18, 1109–1130, https://doi.org/10.5194/os-18-1109-2022, 2022.

Wen, J., Wang, Y., Wang, W., Jezek, K., Liu, H., and Allison, I.: Basal melting and freezing under the Amery Ice Shelf, East Antarctica, Journal of Glaciology, 56, 81–90, https://doi.org/10.3189/002214310791190820, 2010.

Yu, J., Liu, H., Jezek, K. C., Warner, R. C., and Wen, J.: Analysis of velocity field, mass balance, and basal melt of the Lambert Glacier–Amery Ice Shelf system by incorporating Radarsat SAR interferometry and ICESat laser altimetry measurements, Journal of Geophysical Research: Solid Earth, 115, https://doi.org/https://doi.org/10.1029/2010JB007456, 2010.